FABRICATION, SIMULATION AND EXPERIMENT OF A ROTATING ELECTROSTATIC SILICON MIRROR WITH LARGE ANGULAR DEFLECTION

CAMON Henri and LARNAUDIE Franck
Laboratoire d'Analyse et d'Architecture des Systèmes, CNRS
7, avenue du Colonel Roche, 31077 Toulouse Cedex 04, France

ABSTRACT

We propose in this paper the complete study of a bulk micromachined silicon micromirror able to tilt up to +/- 20° at a relatively high frequency (1 kHz). These structures actuated with particular electrodes could be also used as a digital micromirror up to 35°. Their behaviours have been tested in term of static and frequency responses. A non-linear phenomenon has been observed at very large angle. The pressure dependence of the quality factor of the microstructure is reported. Lifetime aspect has also been tested.

INTRODUCTION

Many movable microstructures have been developed in recent years owing to surface and bulk micro machining technologies. The surface micro machining allows monolithic integration of micromirrors arrays for projection displays [1,2,3], single micro mirror [4,5] or mirrors driven by combdrive actuators [6]. All these microstructures have a too small deflection angle and/or reflective area for single laser beam devices. The bulk micromachining is the best way to fabricate mirrors with a relatively large optical area allowing large angle deflection. Nowadays, most of these micromirrors are actuated through planar electrodes [3,7]. However, some papers show that the use of non-planar electrodes increases the electrostatic interaction and consequently reduce the driving voltage [8,9,10,11]. Our application requirements (large angles, low driving voltage, high natural frequency and minimum rise time), cannot be fulfilled with structures described in literature.
Mirrors we have developed are actuated by electrostatic and go to make up the deflection part of the telemetric system of a 3D-laser camera for robotic application, ruling out the possibility of using digital mirrors. The deflection of the laser beam is obtained with two separately actuated crossed 1D micromirrors.

SIMULATION

Operation principle

Two torsion beams suspend the optical reflective plate. A voltage applied between the mirror and the electrodes located below the mirror allows the structure to tilt around the beams. The classical equation of motion of the system is:

$$I\frac{d^2\theta}{dt^2}+\eta\frac{d\theta}{dt}+M_r=M_e \qquad (1)$$

where θ is the tilting angle, I the moment of inertia, η the damping factor, M_r the mechanical restoring torque of the torsion beams and M_e the electrostatic torque.

Mechanical torque

Using the theory of torsion [12] and taking into account the anisotropy of mechanical properties of silicon, we obtain for small tilting angle a linear restoring torque as below.

$$C_{44}\frac{\partial^2\Omega}{\partial x^2}+C_{55}\frac{\partial^2\Omega}{\partial x^2}+2C_{45}\frac{\partial^2\Omega}{\partial x\partial y}=2C_{45}^2-2C_{44}C_{55} \qquad (2)$$

with $\Omega=0$ on (Γ).

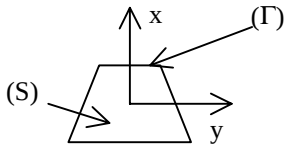

Beam section

C_{ij} are the elastic coefficients of single crystal silicon. To solve (2) we have to transform the C_{ij} coefficients into the crystallographic orientation defined by the torsion beam orientation into the wafer.

$$K=\frac{\left(2\iint_{(S)}\Omega(x,y)dxdy\right)}{l} \qquad (3)$$

$$M_r=2K\theta \qquad (4)$$

where K and l are respectively the stiffness and the length of each beam.

Electrostatic torque

The electrostatic torque is very dependent of the shape of electrodes. Most of them are planar [3,7]. Solving Laplace equation leads to electrostatic torque for planar electrodes [13] (Figure 1):

$$M_e = \frac{\varepsilon_0 V^2 L}{2\theta^2}\left[\ln\left(\frac{x-\frac{D}{2}\sin\theta}{x\cos\theta - d\sin\theta}\right) + \frac{x}{x-\frac{D}{2}\sin\theta} - \frac{x}{x\cos\theta - d\sin\theta}\right] \quad (5)$$

L is the length of the mirror.

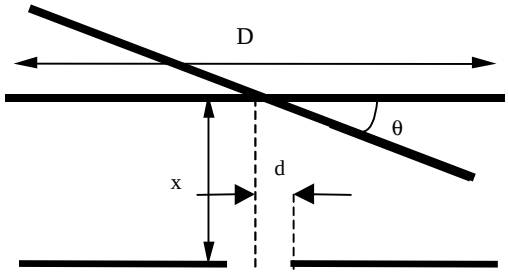

Figure 1: Planar electrodes

Moreover some papers show that the use of non-planar electrodes increases electrostatic interaction and consequently reduce the driving voltage [8,9,10,11]. That's why we developed a model for inclined electrodes. We obtain [9] (Figure 2):

$$M_e = \frac{\varepsilon_0 V^2 L}{2(\alpha-\theta)^2}\ln\left(\frac{x}{d\sin\alpha}\right) \quad (6)$$

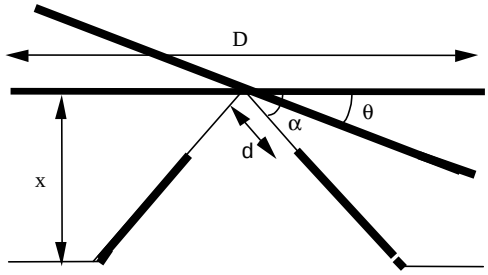

Figure 2: Inclined electrodes

Figure 3 shows the behaviour of two microstructures that are only different by the shape of electrodes. The geometrical characteristics are the characteristics of the structures later exposed in this paper. The advantage of inclined electrodes is clear and confirms the initial choice.

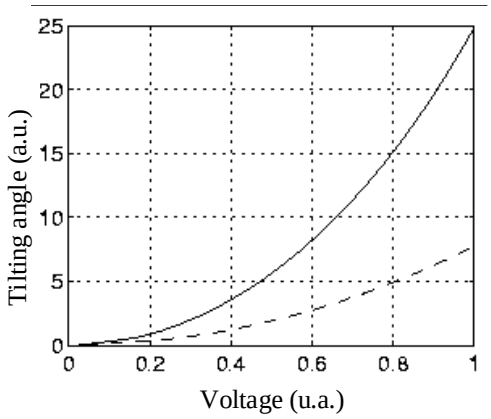

Figure 3: Steady-state response (line: inclined electrodes, dashed line: planar electrodes)

Damping factor

Factors that give rise to energy losses are: support loss, internal friction and air damping.

Most of the support loss appears by friction of assembled piece or grain boundaries [14]. As our microactuator is a single silicon bulk micromachined single piece, damping by support loss can be neglected.

The internal friction of microresonator is due to the thermoelastic effect which has its origin in the strain distribution in the beams. In our case the type of deformation, shear force, does not produce such damping [15].

The air damping is composed of two parts: the viscous force in free space and the squeeze film effect du to the air gap between the movable mirror and the fixed substrate. The viscous force must be calculated using fluids mechanics (Navier-Stokes equation). Some papers purpose an approximation of this damping for cantilevers in bending mode. The squeeze film damping is also estimated in the case of micromirrors with small tilting angles and constant gap [16]. These studies are not applicable to our case: plate in torsional mode, large tilting angle and particular geometry of gap. For the moment we have not succeed in parameterizing the damping factor by modelling. We actually determinate its value by experiment and by fitting the results of simulation with this value. In order to obtain this fit, we have to take into account the exact experimental apparatus in the simulations in order to use as simulated experiment. We decided to choose SABER software to simulate the circuit command as well as the microstructure (Figure 4). Verification of the electrostatic, mechanical and inertial parts of the modelling is tested for each micromirror in a vacuum chamber (at pressure equal to 10 Pa) to reduce the influence of the damping factor. Then, we can recover the values of the damping factor at each pressure conditions.

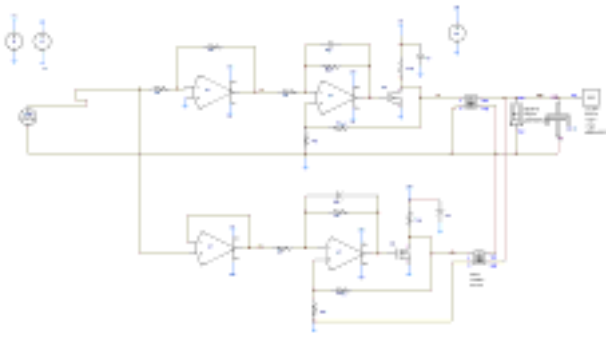

Figure 4: SABER simulation of the mirror and the command circuit

TECHNOLOGY

General overview

The device is made up of two separately building parts: the single crystal silicon mirror-plate suspended by two torsion beams and the electrodes located below the mirror and on each side of the torsion beams axis (Figures 5 and 6).

Process of electrodes

The inclined electrodes are realised using a (110) silicon wafer. By an adequate anisotropic etching (KOH, 85°C, 35% w.), inclined planes with angle of 35 degrees are obtained. A thermally grown SiO_2 layer is used for electrical insulation between the silicon substrate and the electrodes. For the electrodes, a 1 µm Al layer is deposited and etched. A LPCVD SiO_2 film protects the electrodes from the outside.

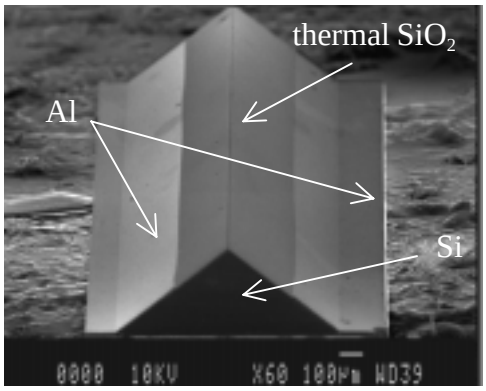

Figure 5: SEM photograph of inclined electrodes

Process of mirror-plate

The mirror and the beams are patterned on the front side by a first anisotropic wet etching (KOH, 85°C, 35% w.) of a (100) silicon wafer. Then a silicon nitride layer is deposited and acts as front side mask during the second wet etching responsible for the release structure from the backside. This layer should be characterised by a high resistance to KOH etch and a low residual stress to prevent the membranes from snapping and the suspended mirrors from breaking during the release. A compromise has been obtained by depositing an 800-nm $SiN_{1.5}$ silicon nitride film. Finally, the Au layer deposited on each side of the wafer is used as reflective film on the front side and as stress compensation layer on the backside. A good fabrication yield of 90% has been obtained for this process.

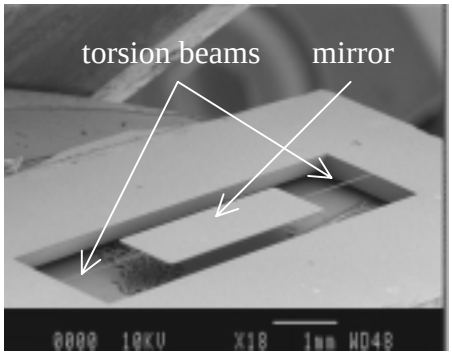

Figure 6: SEM photograph of micromirror and beams

Packaging

We chose to glue the two parts on an insulator substrate with films calibrated in thickness. The electrical connection is done by the backside of the device to increase compactness. Each electrode and the mirror are connected by wire bonds (Figure 7).

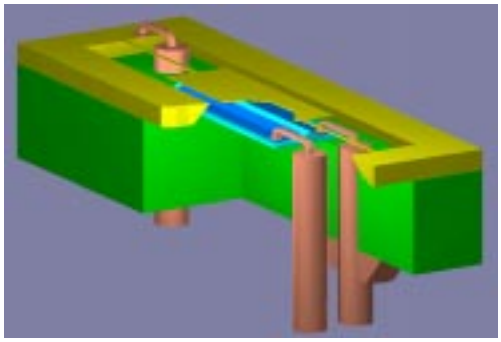

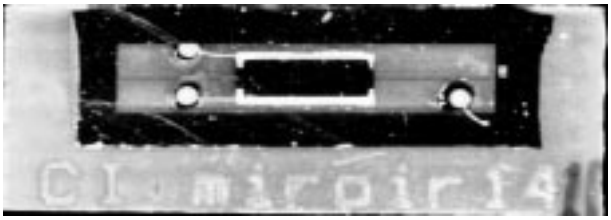

Figure 7: Schematic (top) and top view photograph (bottom) of the packaged device

First, holes are made in the substrate in order to put connectors. Then, electrodes are glued to the substrate and the connections are made. The same operations are done for the mirror part. The alignment of the electrode and the micromirror is realised by using a longer bottom part allowing to put in coincidence the spring and the ridge of the electrodes.

EXPERIMENT

The signals that are fed to the electrodes are produced by a PCB implemented modulator. The modulator is supplied by a constant high voltage source.
The angle measurement is obtained by an optical system. A laser beam is focused on the mirror and then reflected to a Positional Sensor Device (photodiodes). The sensor produces four currents from which the position of the laser spot in the cartesian coordinate frame of the surface is calculated. This position is represented in the form of two voltages.

Static and dynamic responses

The Table 1 indicates that the beam width is 6 μm. As the beam is obtained by KOH etching the cross-section is trapezoidal and the dimension of the beam base is approximately 27 μm.

Table 1: Geometrical characteristics of the microstructure (dimensions in μm)

	Mirror	Beam
Length	3000	2000
Width	1000	6
Thickness	15	15

Figure 8 shows a quite good agreement experiment/model for structure whose geometrical characteristics are described in Table 1. The optical deflection is twice the mirror tilting angle in the case of static analysis and four times in the case of frequency response.

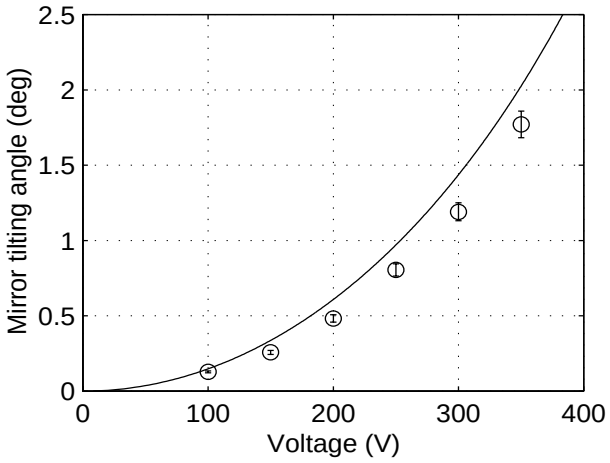

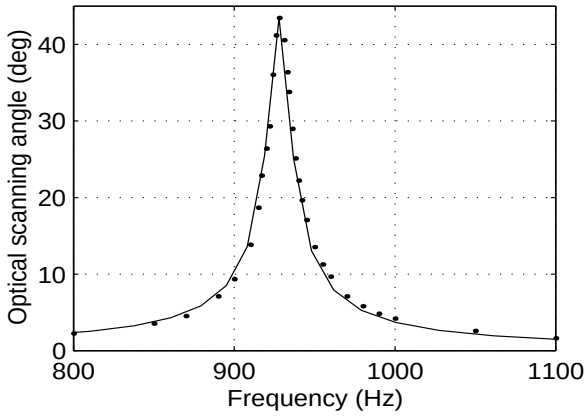

Figure 8: Static (top) and frequency (bottom) response, lines: model, dots: experiment

For voltage amplitude of 140 V, we obtain an optical scanning angle of 43° at the natural frequency 925 Hz. This resonator has a quality factor Q=70 which leads to a damping factor of $\eta=13.10^{-12}$ Nm/rad at the atmospheric pressure.
Figure 9 shows the response to a step load driving voltage of 150 V: a rise time of some tens of milliseconds is observed for a deviation of 0.25°. The addition of a close-loop command reduces this value to 5 ms.

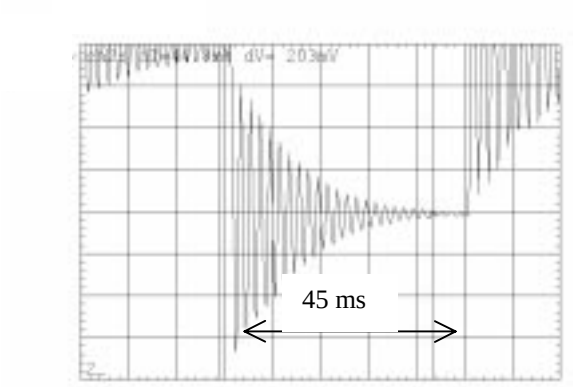

Figure 9: Experimental response to step load-driving voltage

Behaviour at very large angle

When the mirror is operated at very large angle, we observe a disymmetry of the frequency response and a shift of the resonance frequency towards the low frequencies. By increasing the driving voltage till tilting angle of 20° (corresponding to a scanning angle of 80°), we obtain the behaviour of the Figure 10. This experience has been done with a mirror whose natural frequency is about 985 Hz at small angles.

This behaviour is not influenced by the pressure avoiding influence of the fluidic aspect.

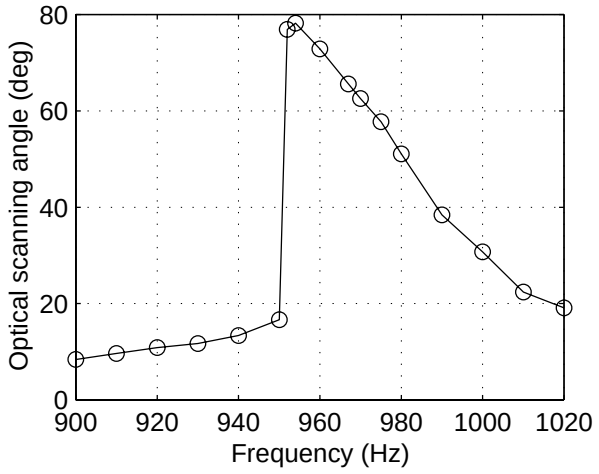

Figure 10: Frequency response for very large tilting angle

This phenomenon could be explained by a "soft" spring restoring force. Adding a non-linear term $K'\theta^3$ ($K' \leq 0$) to the restoring torque (7) leads to such behaviour [17].

$$M_r = 2(K\theta + K'\theta^3) \qquad (7)$$

This type of curve was obtained in simulations with SABER software replacing the linear term by a non-linear restoring torque.
Moreover, operating at more than 20°, the mirror is becoming electrostatically unstable resulting in a collapse condition where a contact between the two parts in formed. By this way we are able to block the structure in a 35° position and obtain a digital micromirror (Figure 11). This can be operated many times without mechanical breakage.

Figure 11: Photograph of a structure blocked at 35°

Experimental variation of quality factor Q versus pressure

Figure 12 shows the pressure dependence (from 10 to 10^5 Pa) of the quality factor. In the molecular region (minor than 10^3 Pa) the experiment are compared with the estimated damping regime. In this region, there is no interaction between gas molecules; therefore, the damping is calculated using kinetic theory of gas [18]:

$$Q = \frac{(2\pi)^{1/2}}{8\pi}\frac{\omega\rho d}{P}\left(\frac{RT}{M}\right)^{1/2} \qquad (8)$$

where ω is the resonance frequency, ρ the density of silicon, d the thickness of the plate, P the pressure, R the universal gas constant, T the absolute temperature and M the mass of a mole of ambient gas. The region 10^3-10^5 Pa is called the viscous region because air acts as a viscous fluid and the drag force must be calculated using Navier-Stokes equation. As we earlier exposed in this paper, we have not calculated the quality factor in this region but it appears that Q is nearly independent of the pressure [18] (Figure 12).

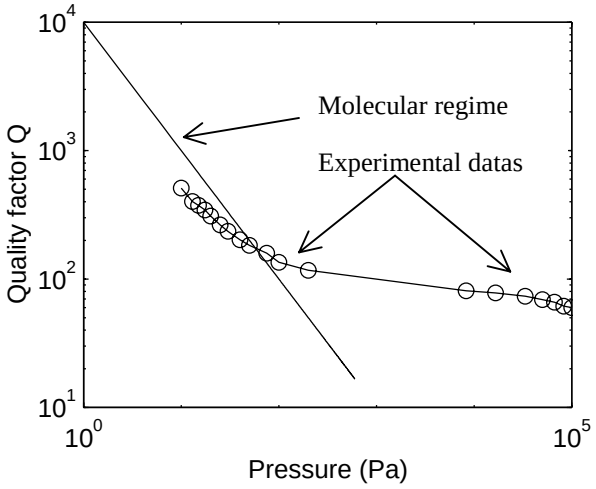

Figure 12: Variation of the Q factor versus pressure

Results of the Figure 12 were obtained with a micromirror whose natural frequency is 790 Hz and with a relatively low driving voltage in order to stay in the linear region. The horizontal shift between experiment dots and the estimated Q in molecular regime is due to the location of the pressure sensor.

Reliability test

We have tested a structure after 600 hours. During this time, the mirror oscillated continuously at its natural frequency with rotation amplitude of +/-10°. By comparison of the frequency response at three different excitation voltages before and after, we have observed a shift of resonance frequencies towards the lowers frequencies because of mechanical fatigue (Figure 13).

More the excitation voltage is high, lower is the shift. The Table 2 indicates experimental values.

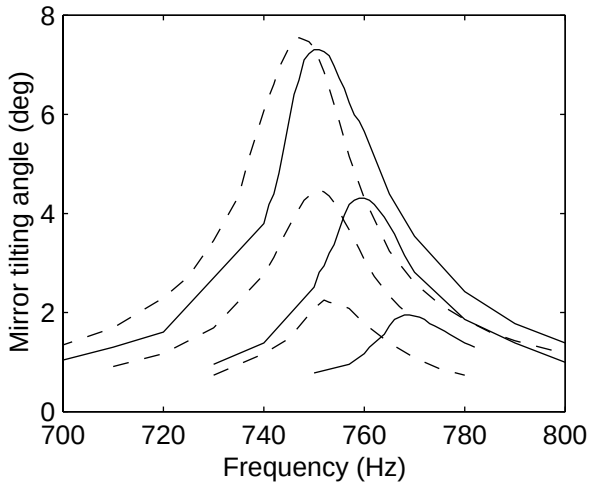

Figure 13: Experimental evolution of frequency response for 3 driving voltages V_0=90 V, 130 V, 170 V. Initial behaviour (line) and after 600 hours (dashed line)

Table 2: Experimental values of shifts

Voltage (V)	Shift (Hz)
90	20
130	10
170	5

CONCLUSION

In this work, we have designed, realised and characterised an electrostatic silicon micromirror with very large angle tilting angle (scanning tilting angle of 80°). The first results show a quite good agreement simulation/experiment. However, works on the alignment of the two glued parts and on the control of beam thickness (the use of SOI would radically solve this problem) are currently driven in order to improve accuracy. Moreover, a complete study should be done on the damping factor to get a complete modelling of the structure. This work must take into account the 3D Navier-Stokes equation.

ACKNOWLEDGEMENTS

The authors would like to thank Monique Dilhan and Thierry Do Conto for their help in the realisation and the packaging of the microstructures. The Microsystems Program of CNRS sponsored this research.

REFERENCES

[1] J. M. Younse, IEEE Spectrum, 27-31, 1993.

[2] C. W. Storment, D. A. Borkholder, V. Westerlind, J. W. Suh, N. I. Maluf, and G. T. A. Kovacs, Journal of Microelectromechanical Systems, Vol. 3, N° 3, 90-96, 1994.

[3] W. Dötzel, T. Gessner, R. Hahn, C. Kaufmann, K. Kehr, S. Kurth, and J. Mehner, 1997 Int. Conf. On Solid-State Sensors and Actuators, Transducers '97, Vol.1, 81-84, Chicago, June 16-19 1997.

[4] M. Fisher, H. Graef, W. von Münch, Sensors and Actuators, A 44, 83-89, 1994.

[5] S-W Chung, J-W Shin, Y-K Kim, and B-S Han, Sensors and Actuators, A 54, 464-467, 1996.

[6] M-H Kiang, O. Solgaard, R. S. Muller, and K. Y. Lau, IEEE Photonics Letters, Vol 8, N° 12, 1996.

[7] W. Lang, H. Pavlicek, Th. Marx, H. Scheithauer, and B. Schmidt, Sensors and Actuators, A 74, 216-218, 1999.

[8] D. Chauvel, N. Haese, P-A Rolland, D. Collard, and H. Fujita, The Tenth Annual International Workshop on Micro Electro Mechanical Systems, 84-89, Nagoya, January 26-30, 1997.

[9] H. Camon, F. Larnaudie, F. Rivoirard, and B. Jammes, Second International Conference on Modelling and Simulation of Microsystems, 628-631, San Juan, April 19-21, 1999.

[10] B. Wagner, K. Reimer, A. Maciossek, and U. Hofmann, 1997 Int. Conf. On Solid-State Sensors and Actuators, Transducers '97, Vol.1, 75-78, Chicago, June 16-19, 1997.

[11] B. Wagner, H. J. Quenzer, S. Hoerschelmann, T. Lisec, and M. Juerss, The Ninth Annual International Workshop on Micro Electro Mechanical Systems, 384-388, San Diego, February 11-15, 1996.

[12] L.D. Landau and E.Lifchitz, Fluid Mechanics, 2nd Ed., New-York, Pergamon, 1989

[13] O. Degani, E. Socher, A. Lipson, T. Leitner, D. J. Setter, S. Kaldor and Y. Nemirovsky, Journal of Microelectromechanical Systems, Vol. 7, N°. 4, December 1998.

[14] H. Hosaka, K. Itao, S. Kuroda, Sensors and Actuators, A 49, 87-95, 1995.

[15] T. V. Roszhart, IEEE Solid State Sensor and Actuator Workshop, Hilton Head Island, 13-16, SC, USA, June 1990.

[16] F. Pan, J. Kubby, E. Peeters, A. T. Tran and S. Mukherjee, Journal of Micromechanics and Microengineering, Vol. 8, 200-208, 1998.

[17] H. J. Pain, The Physics of Vibrations and Waves, Wiley, Chicester, 3rd ed., 1983.

[18] Z. Kadar, W. Kindt, A. Bossche, J. Mollinger, Sensors and Actuators, A 53, 299-304, 1996.